

Presented at the 1981 IEEE  
Nuclear Science Symposium  
Oct. 21-23, 1981, San Francisco.  
To be published in the IEEE  
Transactions on Nuclear Science  
June, 1982

LBL-13862

LBL--13862

DE82 013005

SIGNAL PROCESSING FOR SEMICONDUCTOR DETECTORS

F. S. Goulding and D. A. Landis

Lawrence Berkeley Laboratory  
University of California  
Berkeley, California 94720 U.S.A.

February 1982

Prepared for the U.S. Department of Energy  
under Contract DE-AC03-76SF0098

DISCLAIMER

This document was prepared for the U.S. Department of Energy by an agency of the United States Government. The U.S. Government is authorized to reproduce and distribute reprints for government purposes not withstanding any copyright notation that may appear hereon. It is understood that any copyright in any article in this document is the property of the author(s) and the U.S. Government is authorized to reproduce and distribute reprints for government purposes not withstanding any copyright notation that may appear hereon. It is understood that any copyright in any article in this document is the property of the author(s) and the U.S. Government is authorized to reproduce and distribute reprints for government purposes not withstanding any copyright notation that may appear hereon. It is understood that any copyright in any article in this document is the property of the author(s) and the U.S. Government is authorized to reproduce and distribute reprints for government purposes not withstanding any copyright notation that may appear hereon.

NOTICE

PORTIONS OF THIS REPORT ARE ILLEGIBLE. It  
has been reproduced from the best available  
copy to permit the broadest possible avail-  
ability.

F. S. Goulding and D. A. Landis

Lawrence Berkeley Laboratory  
University of California  
Berkeley, California 94720 U.S.A.ABSTRACT

This is a tutorial paper designed to provide a balanced perspective on the processing of signals produced by semiconductor detectors. The general problems of pulse shaping to optimize resolution with constraints imposed by noise, counting rate and rise time fluctuations are discussed.

I. INTRODUCTION

Many papers and textbooks have been written dealing with our subject. For the purpose of this Short Course on Semiconductor Detectors we are faced with the task of summarizing this mass of material in a short presentation. Clearly such a task is impossible; therefore we have chosen to construct a skeleton of the principal factors involved in optimizing the signal processing channel associated with semiconductor detectors and, using this skeleton, to provide a balanced perspective on the various pulse shaping methods so that our readers can make good judgments about the best solution to their own problems.

Figure 1 shows the basic elements of the pulse processing system. A reverse-biased detector detects single radiation events (photons or charged particles) and produces impulses of current (i.e., charge) into a preamplifier. In practically all cases a charge-sensitive stage (i.e., a capacitively fed-back operational amplifier) is used in the preamplifier so each event in the detector results in a step waveform at the preamplifier output. In some preamplifiers a resistor is used across the feedback capacitor, so a slow decay occurs in the output voltage after the step; in others the charge built up on the capacitor is removed by a pulsed-reset method.

Signals from the preamplifier pass to a main amplifier (sometimes called a pulse or linear amplifier) where pulse shaping is performed primarily to optimize the signal/noise ratio in the signal path. As will be indicated later, other factors may influence the design of the shaper. In all cases, the shaping consists of differentiating and integrating elements that result in a rather narrow pulse compared with the decay time in the preamplifier signal. In the simplest signal processing systems the amplifier output pulse feeds a pulse-height analyzer (PHA) where the amplitude spectrum of the pulses is determined. In general the pulse amplitude is linearly related to the energy absorbed due to an event in the detector, so the amplitude spectrum is essentially an energy spectrum and the effects of noise in spreading the pulse amplitude appear as degradation of the energy resolution of the system.

The simplest system is rarely employed; more commonly other criteria are imposed on signals before performing analysis on them. Such criteria might include setting upper and lower amplitude limits, requiring coincidence with signals in other measuring channels, etc. Figure 1 illustrates the almost universal requirement to reject signals where overlap

within the pulse width of the shaper causes accidental pile-up. These are usually rejected by providing a parallel fast channel where signals are differentiated to produce very short impulses; the train of impulses is then inspected and, when pairs of impulses are too close together, signals in the slow amplitude measuring channel are rejected. In practice the pile-up rejector generates a "valid" signal for signals not subject to pile-up and this valid signal gates the main channel to produce a narrow rectangular signal to feed the pulse-height analyzer.

The elements we have discussed here represent the essential parts of any signal processing system for semiconductor detector signals. We will now discuss each part in more detail.

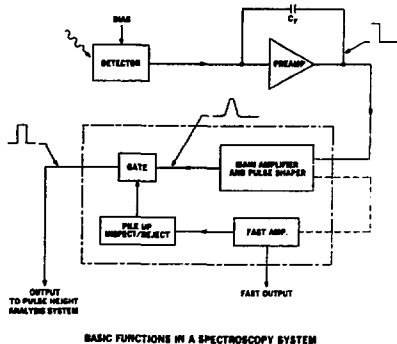


Fig. 1. Basic functions in a spectroscopy system.

II. SEMICONDUCTOR DETECTORS - THE SIGNAL SOURCE1. SIGNAL MAGNITUDE

For practical purposes, the signal produced by a semiconductor detector is proportional to the absorbed energy. Thus:

$$Q = Eq/c \quad (1)$$

where Q is the charge produced (Coulombs)

E is the absorbed energy (eV)

q is the electronic charge ( $= 1.6 \times 10^{-19}$  Coulombs)

$\epsilon$  is the average energy required to produce a hole-electron pair (eV/hole-electron pair)

The value of  $\epsilon$  (which represents the effective conversion efficiency of the detector) depends on details of the interaction mechanisms in the detector material. Not all the incident energy is used producing ionization (which gives us signals)—some is wasted in producing vibrations in the crystal lattice and we cannot recover this energy. Therefore,  $\epsilon$  depends on the material and to a minor degree ( $\sim 0.02$  /°C) on the temperature. We have

Si: 3.61 eV at 25°C ; 3.81 eV at 77°C

Ge: 2.96 eV at 77°C

Compounds (e.g., Hg<sub>2</sub>I, Cd Te): > 4 eV

Therefore germanium detectors produce ~ 20% more signal than silicon detectors for a given energy absorption. However, this is not the only factor in choosing detectors.

## 2. SIGNAL FLUCTUATIONS

The fact that the incident energy is used in both ionizing processes and in exciting vibrational (phonon) modes of the lattice and that such sharing of losses is random means that the signal output charge (which is produced only by ionization) is intrinsically subject to random fluctuations. If the ionizing collisions were very rare compared with the phonon collisions the variance (i.e., RMS fluctuation) in the number N of electron/hole pairs produced would obey simple Poisson statistics:

$$\text{Variance} = \sqrt{N} = \sqrt{E/\epsilon}$$

Since each pair, on the average, corresponds to the absorption of  $\epsilon$  eV in energy we can write:

$$E_{\text{RMS}} = \epsilon \sqrt{N} = \sqrt{E\epsilon}$$

The full width at half maximum (FWHM) energy resolution  $E_{\text{FWHM}}$  would therefore be:

$$E_{\text{FWHM}} = 2.35 \sqrt{E\epsilon}$$

In practice our assumption about the rarity of ionizing collisions is incorrect and this produces a reduction in  $E_{\text{FWHM}}$ . We write:

$$E_{\text{FWHM}} = 2.35 \sqrt{FE\epsilon} \quad (2)$$

Where F is the Fano factor, which is always less than unity and is typically approximately 0.12 for silicon and germanium. It is difficult to assign a value to F for other materials because the statistics of trapping effects hides the charge production fluctuations in any practical measurement.

The values of the intrinsic detector resolution for silicon and germanium detectors as a function of energy are given in Table 1.

Table 1. Energy Resolution vs Energy (Si and Ge)

(Fano Factor = 0.12)

Energy	$\Delta E_{\text{FWHM}}$ (eV)	
	Si	Ge
1 keV	50	44
2	70	62
5	111	99
10	157	140
20	222	198
50	351	313
100	496	442
200	701	626
500	1109	990
1 MeV	1568	1401
2	2217	1980
5	3506	3132
10	4960	4420
20	7010	6260
50	11090	9900
100	15680	14010
200	22170	19800
500	35060	31320

## 3. SIGNAL SHAPE

While the ionization in a detector is produced in a very short time compared with any of the shaping times we employ, the charge must be collected by virtue of electrons and holes drifting from their point of origin to the electrodes on the detector. The time taken for this process may, under some circumstances, influence the choice of signal shaping method to be used. We will discuss a few elementary cases remembering that our emphasis here is on amplitude measurements. The case of semiconductor detectors used for fast timing purposes, where the charge collection process can be very important, is dealt within an accompanying paper by H. Spieler.

## A. Planar Detectors

For the purpose of this discussion we will assume that the material used to fabricate the detectors is extremely pure so virtually no (net) acceptors or donors exist in the detector material. This simplifies our picture in that the electric field due to applied bias is constant throughout the material between the electrodes. This is not always the case and, where it is not, it is obvious that longer collection times will result from low field regions.

Figure 2a shows a planar geometry detector and indicates the production of a single hole-electron pair at a distance x from the p<sup>+</sup> contact of the detector (an accompanying paper by E. Haller discusses the

fabrication and operation of detectors). The electron drifts in the applied electric field toward the positively-biased n<sup>+</sup>-contact while the hole drifts to the opposite contact. The external signal current due to movement of a carrier (hole or electron) persists while the carrier is moving and stops when the carrier is collected. Thus, if we assume that electrons move at a velocity  $v_e$  and holes at  $v_h$ , the charge collected as a function of time will be as shown by the solid line in Fig. 2b. The dotted lines show the behaviour for hole-electron pairs produced at various values of  $x$ . Note that the total signal due to each pair is the electronic charge  $q$  and the electron movement contribution is larger when the electron travels further than the hole and vice-versa. The maximum collection time (and therefore maximum rise time of the signal) is the electrode to electrode transit time of the slowest carrier (always holes). In practice, the signal observed for a given radiation event is the integral of the signals for all electron hole pairs produced by the event. For low-energy photons, where the electron-hole pairs are produced essentially at one point, the general form of the signal will be that of the solid line in Fig. 2b. For charged particles, where electron-hole pairs are produced along the particle track, a more complex signal shape results.

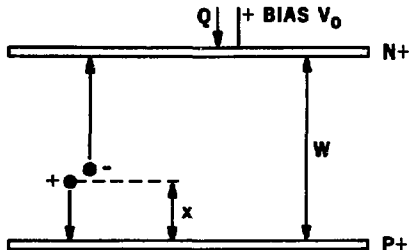
The velocities of the carriers and, therefore, the time scale associated with Fig. 2b are determined by the basic transport mechanisms for carriers in the material, by the electric field and by the temperature. A very simple case occurs for high electric fields and low temperatures (typically of all liquid-nitrogen cooled silicon and germanium detector systems). Here the velocities of both holes and electrons saturate at a constant velocity near  $10^7$  cm/s. Therefore, for the case of a planar detector (as seen in Fig. 2a) 1 cm thick the maximum rise time is 100 ns and, for events producing ionization only at the middle of the detector, 50 ns is the total collection time.

For detectors used at room temperature and reasonable bias (such as the common use of lithium-drifted silicon detectors in studies of nuclear reactions at accelerators) the velocity of the carriers is proportional to the electric field:

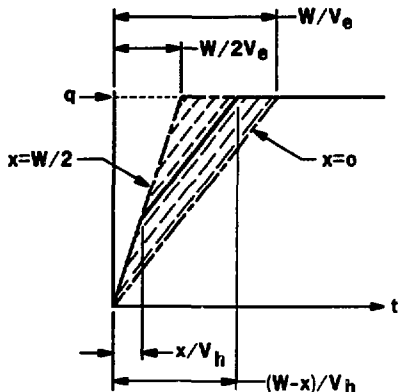
$$\begin{aligned} v_e &= \mu_e E \\ v_h &= \mu_h E \end{aligned} \quad (3)$$

where  $\mu_e$  and  $\mu_h$  are called the electron and hole mobilities. Approximate values of these mobilities in  $\text{cm}^2 \text{V}^{-1} \text{s}^{-1}$  at room temperature are:

$$\begin{aligned} \mu_e &= 1250 \text{ (Si)} : 3600 \text{ (Ge)} \\ \mu_h &= 450 \text{ (Si)} : 1600 \text{ (Ge)} \end{aligned} \quad (4)$$



A.



B.

XBL 822-7912

Fig. 2. The pulse shape generation in a planar detector.

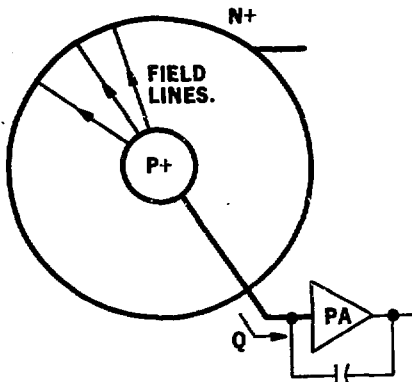
These mobilities rise rapidly as the temperature is reduced because the thermal vibrations of the lattice, which interfere with carrier movement, are reduced. An example of a detector operating in the domain where carrier velocities are proportional to the electric field might be that of a 5 mm thick lithium-drifted silicon detector operated at room temperature with 500 V applied. In this case the electric field is 1000 V/cm and the carrier velocities are  $v_e = 1.25 \times 10^6$  cm/s and  $v_h = 0.45 \times 10^6$  cm/s. The maximum carrier collection time is therefore slightly greater than 1  $\mu$ s. It should be obvious in this case that the use of shaping involving  $< 1$   $\mu$ s differentiation results in loss of signal. Furthermore, since particles with different ranges produce signals with different rise times in the detector, the use of short pulse-shaping times results in output signals that are not linear with absorbed energy. This ballistic deficiency effect must be borne in mind in charged-particle applications of thick detectors.

### B. Coaxial Detectors

A very common germanium detector geometry is the coaxial arrangement shown in Fig. 3. This type of detector is used universally for high-efficiency, high-energy gamma-ray spectroscopy and, since large volumes are essential, the diameter may be quite large—up to 6 cm being typical. The central p-type core in a lithium-drifted germanium coaxial detector is usually of small diameter (typically 0.5 cm) and a similar diameter is employed for the central "cut-out" cylinder in high-purity germanium detectors. The non-uniform field distribution produced by this geometry and the long carrier transit distances result, generally, in low fields near the outside and long charge collection times. Depending on where a gamma-ray interacts, collection times over  $\sim 1$   $\mu$ s may occur.

With the polarity shown in Fig. 3, a positive potential is present on the periphery of the detector; since the largest part of the detector volume is near the outside, the great majority of interactions occur in these regions. Since, with this polarity, the signals are dominated by hole collection, they tend to be quite slow. A reverse polarity detector (negative voltage on an  $p^+$  peripheral region) is better in this respect; both polarities are available in high-purity germanium detectors but only the polarity shown in Fig. 3 is obtainable in lithium-drifted detectors. A substantial advantage in respect to the trapping produced by radiation damage also results from the reverse polarity because the traps produced by radiation damage are dominantly hole traps.

The lesson to be learned from this picture is that the type of pulse shaping used in the signal processing path must be tolerant of rise time fluctuations in the detector signal, particularly when large coaxial detectors are used. Significant pulse amplitude fluctuations due to variable charge collection in the detector (known as ballistic deficiency effects) cannot be tolerated. Since the detector charge production statistics (see Eq. 2) are proportional to  $\sqrt{E}$  while ballistic deficiency effects are essentially proportional to  $E$ , it is obvious that the latter effects may be very important at high energies.



XBL 822-7913

Fig. 3. Coaxial detector geometry. The polarity may be reversed in high-purity germanium detectors.

### 4. LEAKAGE CURRENT

A detector is, for electrical purposes, a reverse biased semiconductor diode and it exhibits a leakage current, whose fluctuations produce noise. A basic source of such leakage is the generation of hole-electron pairs in the bulk of the detector material by thermally induced lattice vibrations. Direct transitions of electrons from the valence to conduction band are rather unlikely compared with two-step transitions via intermediate trapping levels and particularly those levels near the middle of the band gap. For this reason the leakage current of semiconductor detectors often obeys the relationship

$$I_L \propto \alpha(-E_g/2kT) \quad (5)$$

where  $I_L$  is the leakage current

$E_g$  is the band gap of the material  
( $\sim 0.7$  eV for Ge;  $\sim 1.1$  eV for Si)

$T$  is the temperature ( $^{\circ}$ K)

and  $k$  is Boltzman's Constant

The leakage current of germanium detectors at room temperature is completely unacceptable. Therefore, all germanium detectors must be used at or near to liquid nitrogen temperature (77 $^{\circ}$ K). While silicon detectors can, and often are, used at room temperature, high resolution applications of these detectors also require cooling (generally to 77 $^{\circ}$ K but not always).

In practical detectors, leakage current produced in surface channels is always dominant. Typical values for silicon detectors range from 10 nA to 10  $\mu$ A at room temperature; both silicon and germanium detectors exhibit leakages in the pA range or less at 77 $^{\circ}$ K.

Since germanium detectors are very sensitive to infrared radiation they must be surrounded by a cold (77°K) shield to reduce leakage to these low values.

We note that charge trapping effects may sometimes make the use of silicon detectors at a temperature greater than 77°K desirable even at the cost of an increase in leakage current. This is particularly true at high energies (such as in beta-ray detectors) since the signal fluctuations (expressed in eV) due to trapping increase as the signal increases, while the signal spread due to noise is independent of energy.

### 5. MISCELLANEOUS DETECTOR FACTORS

Although other detector effects generally do not influence signal processing, trapping effects (see the last paragraph) and contact resistance can sometimes result in problems. We will not dwell further on these in this paper.

## III. THE PREAMPLIFIER

### 1. COUPLING TO THE DETECTOR

Figure 4 shows the two methods commonly used to couple detector signals to the preamplifier input. For all high resolution (low-temperature detector systems) the dc coupling method is used primarily because it minimizes the stray capacitance in the input circuit, thereby improving the signal/noise ratio.

Another slight advantage of this method is that the preamplifier output can be monitored to measure the leakage current of the detector. In pulsed reset systems (see the Introduction), the reset rate combined with the value of  $C_F$  provides an absolute measurement of the leakage current; in resistor/capacitor feedback systems the dc level at the preamplifier output, and its change as the detector bias voltage is increased from zero to its proper value, is a good measure of detector leakage current. The fact that neither electrode of the detector is at ground potential does result in slight inconvenience in the mechanical design of detector mounts but this is usually more than offset by the advantages of the dc connection.

The ac connection shown in Fig. 4 is commonly employed with room temperature detectors used in charged particle spectroscopy. In this arrangement one side of the detector is conveniently grounded. However, the detector load constitutes an additional noise source, the stray capacitance to ground worsens the signal/noise ratio and the extra differentiator formed by the coupling capacitor, detector load and preamplifier input may cause degradation of resolution at high counting rates. Where high-energy charged particles are being detected, these factors may contribute less to resolution than various detector and beam resolution factors; therefore, the ac coupled arrangement is generally satisfactory for these applications.

### 2. NOISE DUE TO SHUNT RESISTANCE IN THE INPUT

The requirement for the highest possible values of shunt impedance in the input circuit often puzzles users of detector systems. Therefore, we will digress for a brief explanation of this result. Figure 5 shows the equivalent input circuit of a detector preamplifier system with an input capacitance  $C$  and a shunt resistance  $R$ . The noise produced by this resistance can be represented as a noise voltage

generator ( $\bar{v}^2 = 4 kTR \Delta f$ ) as shown in the figure.

Across the input capacitance  $C$ , the noise voltage is given by:

$$\bar{V}_{out}^2 = 4 kT \Delta f \left( R / (1 + 4\pi^2 f^2 C^2 R^2) \right) \quad (6)$$

where  $k$  is Boltzmann's Constant  
 $T$  is the temperature (°K)  
 $f$  is the frequency  
 and  $\Delta f$  is a small bandwidth interval centered on  $f$ .

To find the total noise at the system output this equation must be integrated over the bandwidth of the shaper amplifier. As  $R$  is increased from zero it is clear that the noise voltage increases to a maximum value when  $R = 1/2\pi fC$  then decreases, becoming proportional to  $1/R$  at large values of  $R$ . The noise is therefore small for very small values of  $R$  and for very large values; in the former case the signal at the input is virtually shorted out so it is obvious that very large values of  $R$  are essential in high-resolution systems.

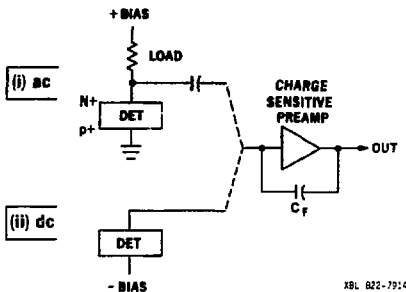


Fig. 4. Coupling the detector to a preamplifier.

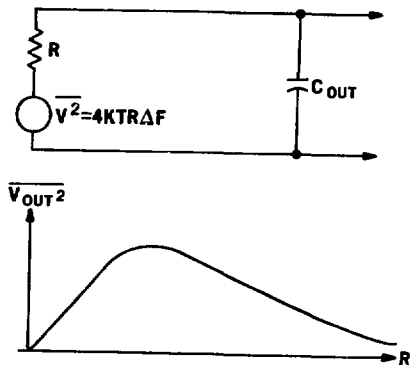
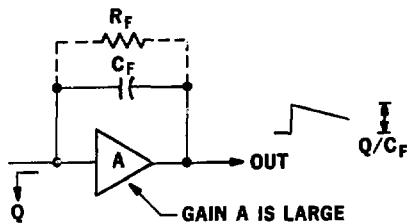


Fig. 5. Input circuit and the behaviour of noise as the value of the shunt resistance is changed.

### 3. THE CHARGE-SENSITIVE CONFIGURATION

The charge-sensitive preamplifier configuration was developed in the early days of semiconductor detectors when the detector capacitance varied with applied voltage. By applying capacitive feedback to the input of a high gain stage, as shown in Fig. 6, the output signal ( $Q/C_F$ ) is made almost totally insensitive to variations in the detector capacitance. In this circuit the input point is a virtual ground and for practical purposes it does not move in potential. Even with modern detectors which are nearly all fully depleted and therefore, to first order, of constant capacitance, small capacitance changes can occur due to changes in detector surface states. Therefore the charge-sensitive configuration is universally employed in modern spectrometers. The feedback capacitor, usually of small value in very high resolution systems, does add to the total input capacitance for the purpose of noise calculations, but this price is acceptable in all cases. In very high-resolution x-ray spectrometers the feedback capacitance value is often less than 0.1 pF and, physically, the capacitance is incorporated in the specially designed front-end FET package.



XBL 822-7916

Fig. 6. The charge sensitive preamplifier configuration.

### 4. RECHARGE METHODS

In Fig. 6, radiation absorbed in the detector and the steady detector leakage current build up the charge on the feedback capacitor  $C_F$  and would cause the preamplifier output to steadily rise until it is saturated. Therefore, means must be provided to discharge  $C_F$ . In many systems this is achieved by a high-valued resistor paralleling  $C_F$  and each step signal at the preamplifier output decays with a time constant  $C_F R_F$  which is usually quite long  $> 50 \mu s$ . Since the further differentiation required in the snaping amplifier would result in a long-term overshwing in the amplifier output with consequent serious effects on resolution at high counting rates, a pole zero cancellation method is used to compensate for the  $R_F C_F$  decay--this is illustrated in Fig. 7. The compensation is achieved by shunting the main differentiator capacitor in the shaping amplifier by an adjustable resistor  $R_1$ . It can be shown that  $R_1$  can be adjusted to exactly compensate for the preamplifier signal decay. In the simple case where  $T_F \gg T$  the correct value of  $R_1$  is given by:

$$R_1 = R_T/T \quad (7)$$

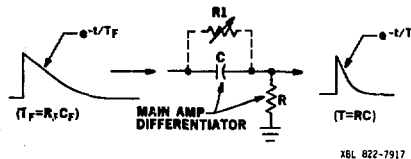


Fig. 7. Pole-zero cancellation circuit.

While this method of recharge is satisfactory for many non-critical spectrometers, the disadvantages of the shunt resistor  $R_F$  are serious limitations in high-resolution high-rate systems. These disadvantages are:

- i) The resistor  $R_F$  acts as a noise source; as indicated in the previous section, use of a very large value of  $R_F$  minimizes this noise contribution.
- ii) The stray capacitance associated with  $R_F$  degrades the signal/noise ratio.
- iii) High-valued resistors do not, in general, behave as pure resistors at the high frequencies ( $\sim 100$  kHz) used in shaping amplifiers. Therefore the pole-zero compensation is never perfect and resolution can be seriously degraded at high counting rates.

For these reasons the pulsed reset methods have been developed to discharge  $C_F$  without the problems associated with resistive discharge methods. Figure 8 shows schematically the most common method used in high-resolution spectrometers. In this technique charge from the detector accumulates on  $C_F$  until the preamplifier output voltage reaches a preset upper level. At this point a limit discriminator fires turning on current in a light-emitting diode whose light is directed onto the input FET. The collector-gate diode of the FET acts as a photodiode so a substantial photocurrent flows into the FET gate, rapidly ( $\sim 5 \mu s$ ) discharging  $C_F$ . When the voltage at the output of the preamplifier reaches a preset lower level the light is turned off and normal operation of the spectrometer starts again. During the brief reset period the pulse-processing system is inhibited.

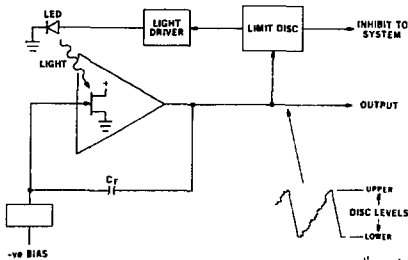


Fig. 8. The pulsed-light feedback method of recharging the feedback capacitor.

The advantages associated with the pulsed-light reset method include:

- i) No added stray capacitance is introduced into the input circuit.
- ii) Since the recharge current flows only during reset, no noise is produced by it during the normal counting period.
- iii) No pole-zero cancellation is needed. Excellent high-counting rate performance is achieved.

Some small disadvantages remain:

- i) The counting time must be extended by a small factor to compensate for the slight loss of time during resets.
- ii) In the circuit shown in Fig. 8, the final input signal that triggers the reset would not be processed; this can be shown to result in a slight spectral distortion. Where this is important, a simple modification can be made to the circuit to permit processing the pulse and delaying reset until such processing is complete.
- iii) Some FETs show small after-effects of the light (and also detectors if they see the light). These after-effects can cause resolution degradation at high counting rates. Careful selection of FETs and proper shielding of the light from the detector eliminates these problems.
- iv) Large pulsed currents (~ tens of mA) are required in the LEDs. These currents can cause ground-loop interactions between the front ends in multidetector systems. For this reason a transistor-reset method has been employed recently in such systems.<sup>1</sup>

## 5. FRONT-END NOISE EQUIVALENT CIRCUITS

It has been traditional to carry out noise calculations in the frequency domain and the equivalent circuit for noise calculations shown in the upper part of Fig. 9 has been commonly used. In this figure we have omitted any parallel resistive component, partly because, as indicated in the previous section, systems often have no parallel resistive component, and partly because the effect of such resistance (if of very large value) can be included in the parallel current noise generator. This noise generator produces the usual Johnson noise:

$$\overline{i_n^2} = 2qI \Delta f \quad (8)$$

The input FET noise is represented by a series voltage noise generator exhibiting Nyquist noise:

$$\overline{e_n^2} = 4kT R_{eq} \Delta f \quad (9)$$

For FETs the equivalent noise resistance that represents fluctuations in the channel current is given by:

$$R_{eq} = A/g_m \quad (10)$$

where the constant A depends on the geometry but is generally approximately unity, and where  $g_m$  is the

transconductance of the FET. In this model the detector signal is treated as a charge Q arriving at the input in a very short time compared with any shaping times used in the processor.

In recent years much noise analysis has been carried out in the time (rather than frequency) domain. Such analysis has the advantage that better intuitive judgements about the effects of shaping can be made in the time domain; the last part of this paper will be devoted to a simple analysis of shapers based on this approach. The lower part of Fig. 9 shows the equivalent input circuit in terms of time behaviour. The detector acts as a step function signal source producing a signal Q/C in size. The parallel current noise generator is pictured as random charge impulses producing random steps across C proportional in size to 1/C. It is immediately obvious that, as far as parallel (or STEP) noise is concerned, the signal/noise ratio is independent of the value of C. The series noise is replaced by a random train of voltage impulses (called DELTA noise). The amplitude of these is independent of the value of C (they are physically due to the FET that follows C), so the signal/noise ratio for delta noise is proportional to 1/C.

We note that this model deals only with the two simple noise terms. Noise coupling to the input via complex elements (such as surface noise in detectors and FETs) cannot be represented so simply. In the aggregate such noise is generally referred to as 1/f noise. We will mention its effect in practical systems in the next sections.

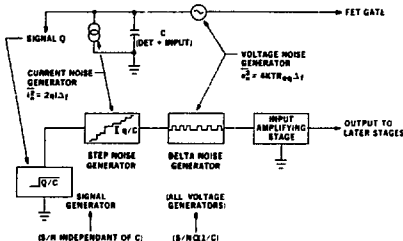
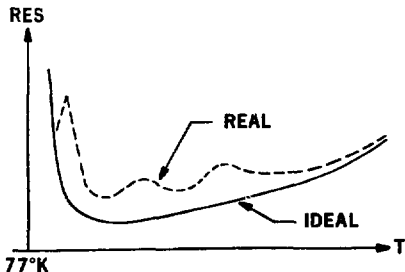


Fig. 9. Input circuit noise sources.

## 6. FIELD-EFFECT TRANSISTORS

Junction field-effect transistors (FETs) are used universally as the input amplifying element in all semiconductor detector spectroscopy preamplifiers. Under normal circumstances adequate gain is provided by this stage to make noise sources in later stages negligible, but choice of low-noise transistors for the elements immediately following the FET is desirable. Since the FET input capacitance contributes to the total input circuit capacitance and the series noise resistance  $R_{eq}$  of Eq. 10 is  $\propto 1/g_m$  it is obvious that a high ratio of  $g_m/C$  is desirable. Since this ratio is directly related to the line width achievable by photo-lithography it is clear that only the most modern FETs are useful in this application. The noise in the FETs should become smaller as the temperature is lowered below room temperature. Other factors involved in the choice and operation of FETs include:

- i) The FET should be selected to have an input capacitance that reasonably matches the detector capacitance.
- ii) The equivalent noise resistance is ideally  $\sim 1/g_m$ . Parasitic series resistance in the gate circuit should always be  $\ll 1/g_m$  if its noise contribution is to be negligible. This is particularly important at short measurement times (where series noise is dominant) and where large detector capacitances are matched by FETs with high capacitance and transconductance.
- iii) In all low-temperature applications, the bumps in the noise cooling curve illustrated in Fig. 10 should be avoided. This is a major factor in the selection of FETs. The bumps are known to be associated with impurity and defect trapping/detrapping effects in the FET channel near to the edge of the gate depletion layer. As is clear in Fig. 10, an optimum operating temperature that is greater than 77°K exists for all FETs. (Freeze out of the main hopant occurs just above 77°K.) The optimum temperature is usually approximately 130°K, and some means for heating the FET to this temperature must be employed.
- iv)  $1/f$  noise may be produced by the FET header and by FET surfaces. It is common to mount FETs for high resolution systems in very low loss packages specially developed for this application.
- v) As the FET drain-gate voltage is increased, impact ionization may occur; in this case the gate, being the most negative point in the FET collects the holes produced and a very noisy gate current results. The voltage onset of impact ionization decreases as the temperature is lowered. Therefore, the operating drain voltage of all FETs should be explored to determine the maximum permissible drain voltage. This is usually very much smaller than the manufacturer's ratings and, in many cases, may only be 2 or 3 volts.
- vi) For pulsed-light reset systems any slow after-effects of the light must be avoided. FETs should be selected to minimize such effects.



XBL 822-7920

Fig. 10. The behaviour of FET noise as the temperature is varied.

### 1. PURPOSES

A trivial and often neglected function of the shaping amplifier is to amplify signals. Furthermore, depending on the application, the gain must be variable by switching and, usually, by a continuous control. In many older amplifiers, gain switching is accomplished by switching an input attenuator; an unfortunate result of this is that the main amplifier input noise may become dominant when the gain is set to a very low value. For this reason it has become common to vary the gain at a number of points in an amplifier, thereby minimizing overload effects while keeping the contributions of main amplifier noise sources to a small value. (This illustrates the problems associated with a unique feature of nuclear and x-ray spectroscopy systems, namely the wide dynamic range. Systems measure energies ranging from less than 1 keV to more than 1 GeV, a range greater than  $10^6:1$ .)

The more sophisticated function of a shaping amplifier is to shape the signals to optimize spectrometer performance. This might involve a compromise between:

- i) Achieving the best possible signal/noise ratio.
- ii) Permitting operation at high counting rates without degrading resolution.
- iii) Making the output pulse amplitude insensitive to rise time fluctuations in the detector signal.

These questions will constitute the main topics in the remainder of this paper.

### 2. INTUITIVE PICTURE OF THE EFFECT OF MEASUREMENT TIME

A quick picture of the behaviour of the signal-to-noise ratio as we vary the time used to measure an event can be gained by assuming that we integrate all information (both signal and noise) for a measurement time  $T_m$ . We then have:

$$i) \text{ Signal out } \propto T_m$$

$$ii) \text{ Delta noise (which corresponds to counting random pulses for a time } T_m) \propto T_m^{-1/2}$$

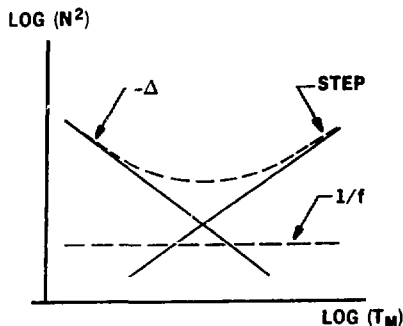
$$\therefore \text{ DELTA NOISE/SIGNAL OUT } \propto T_m^{3/2} \quad (11)$$

$$iii) \text{ Step noise (both the random counting factor and the integration of charge occur) } \propto T_m^{3/2}$$

$$\therefore \text{ STEP NOISE/SIGNAL OUT } \propto T_m^{1/2} \quad (12)$$

These relationships are illustrated in Fig. 11. They apply to all shaping networks; that is, if the shape is kept constant while times are scaled, the  $(\text{delta noise})^2$  is proportional to the reciprocal

of the time scale and the (step noise)<sup>2</sup> is proportional to it. As is clear in Fig. 11, from the point of view of signal/noise only, an optimum measurement time must exist. In practice, other constraints, such as the need to operate at high counting rates or the need to reduce microphony effects, may force operation at a measurement time that is shorter than the optimum from a signal/noise point of view. Finally in Fig. 11 we show the effect of 1/f noise. This noise term has a generally flat behaviour with measurement time. Its effect is to flatten the noise minimum and substantially increase the total noise (terms must be added in quadrature) in the region of the noise minimum. The proportions shown in Fig. 11 are fairly representative of many systems and the noise minimum generally occurs in the range 5 to 100  $\mu$ s depending on the particular type of spectrometer.



XBL 822-7921

Fig. 11. Generalized noise behaviour of a system as the measurement time  $T_m$  is varied.

## 2. SIMPLE RC INTEGRATOR, RC DIFFERENTIATOR SHAPER

As is obvious from the foregoing discussion the shaper must contain some type of integrator to cut out the high frequency or delta noise and a differentiator to cut out the low frequency step or parallel noise. The simplest shaper consists of an RC differentiator and an RC integrator of equal time constant. This combination serves to limit both low and high frequency noise and also provides a pulse of limited duration (a few times RC) which allows a finite pulse rate without pile up. The output pulse may easily be shown to peak at a time equal to the RC time constant.

The following analysis of this type of shaper in the frequency domain illustrates the general nature of the calculation. Figure 12 will be used in this analysis; it consists of a voltage sensitive amplifier\* whose shaping function is represented by the gain-frequency function  $G(f)$ . Neglecting the effects of the RC differentiator and integrator that determine  $G(f)$ , we assume a dc gain of unity in the amplifier. It is easy to show that the peak height  $P_0$  of the RC differentiated and integrated output pulse is

equal to  $(1/e)$ , if the two RC time constants are equal in value. The value of the gain function  $G(f)$  is given by

$$G(f) = 2\pi f \tau_0 / (1 + 4\pi^2 f^2 \tau_0^2) \quad (13)$$

we have:

$$\text{Signal Out for 1 Electron-Hole Pair} = q/Ce \quad (14)$$

$$\begin{aligned} \text{Total noise}^2 \text{ due to } \Delta t &= \overline{\Delta^2} \\ &= \int_0^\infty 4 kT R_{eq} \{G(f)\}^2 df \end{aligned}$$

$$\therefore \overline{\Delta^2} / \text{Signal}^2 = \frac{4 kT R_{eq} C^2 e^2}{q^2} \int_0^\infty \{G(f)\}^2 df$$

Also: (15)

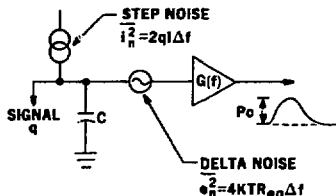
$$\begin{aligned} \text{Total noise}^2 \text{ due to steps} &= \overline{S^2} \\ &= \int_0^\infty \frac{2qI}{4\pi^2 f^2 C^2} \{G(f)\}^2 df \end{aligned}$$

$$\therefore \overline{S^2} / \text{Signal}^2 = \frac{e^2 I}{2\pi^2 q} \int_0^\infty \frac{\{G(f)\}^2}{f^2} df \quad (16)$$

Substituting from Eq. 13 in Eqs. 15 and 16 yields the results:

$$\overline{E_L}^2 = \frac{kT C^2 \omega^2 R_{eq}}{2q^2 \tau_0} = \frac{\pi T C^2 e^2}{2q^2 \tau_0 g_m} \quad (\text{for FET}) \quad (17)$$

$$\overline{E_S}^2 = \frac{I e^2 \tau_0}{4q} \quad (18)$$



XBL 822-7922

Fig. 12. Frequency-domain analysis of a system.

\*This is done to simplify the calculation; the result is virtually the same for a fed back configuration in keeping the general rule that feedback can only worsen the S/N ratio but that such degradation can be kept very small.

In these equations  $\overline{E_A^2}$  is the mean squared delta noise expressed in terms of equivalent collection of

hole-electron pairs in the detector and  $\overline{E_C^2}$  is the mean squared step noise expressed in the same terms. We note, as expected from the previous section,

that  $\overline{E_A^2} \propto \tau_0^{-1}$  and  $\overline{E_C^2} \propto \tau_0$ . Figure 13 shows the calculated behaviour with varying RC time constant  $\tau_0$  assuming an input capacitance of 5 pF, a parallel current term (detector leakage) of  $10^{-13}$  A and a transconductance of 5 mA/V. The left ordinate shows the noise expressed in hole-electron pairs (N) while the equivalent energy resolution for a silicon detector is shown on the right ordinate. The behaviour shown in Fig. 13 is fairly representative of such a detector system although some 1/f noise would usually also be observed.

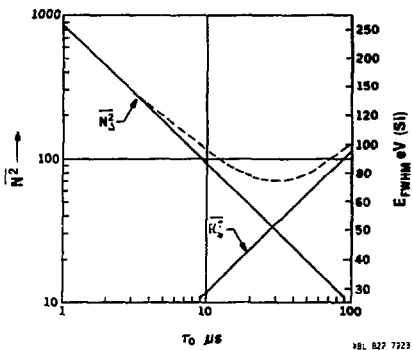


Fig. 13. Calculated noise behaviour of a system with  $C = 5$  pF,  $I = 10^{-13}$  A,  $g_m = 5$  mA/V using a simple RC-RC shaper.

#### 4. COMPARING PULSE SHAPES - TIME DOMAIN ANALYSIS

It is obvious that analysis in the frequency domain gives no intuitive insight into the pulse shape features that affect the signal/noise ratio or those that may affect pile up at high counting rates. Furthermore, systems (called time-variant) have been developed which involve switching the values of circuit elements in synchronism with signals. Such systems cannot be analyzed in the frequency domain. These factors have led in recent years to increased use of methods of analysis in the time domain. With such methods it becomes possible to more simply appreciate the effects of certain features in pulse shapes that control noise and the signal/noise ratio.

The methods are based on the simple fact that a noise step occurring at a time  $t$  before the time at which we measure a signal (see Fig. 14) leaves a residual  $R(t)$  at the measurement time. The effect of all noise steps prior to the measurement time is the result of summing all noise steps prior to the measurement time. For any given signal, of course, the result of prior noise steps may be positive or negative and may have a wide range of amplitudes; we are concerned with the mean square fluctuations in the noise at the signal measurement time. To obtain

this we integrate the effect of all prior noise steps:

$$\text{Total Step Noise}^2 \propto \int_0^{\infty} \{R(t)\}^2 dt$$

where  $R(t)$  is the effect of a noise step prior at time  $t$  to the measurement time.  $R(t)$  obviously depends on the type of shaper employed and, for passive (i.e., not time variant) filters, the effect of a noise step is the same as the step response of the shaper. The shaper also affects the signal magnitude so it is reasonable to consider the effect of a shaper in terms of an index:

$$\text{Step Noise Index} = \overline{N_s^2} = (1/S^2) \int_0^{\infty} \{R(t)\}^2 dt \quad (19)$$

Delta noise can be considered in the same way. Since a delta impulse is equivalent to two equal opposite polarity steps spaced by an infinitesimally small time, the effective delta noise residual function is the differential of  $R(t)$  (i.e.,  $R'(t)$ ) and the delta noise index is given by:

$$\text{Delta Noise Index} = \overline{N_A^2} = (1/S^2) \int_0^{\infty} \{R'(t)\}^2 dt \quad (20)$$

It is important to realize that the noise behaviour of any shaper can be simply represented by Eqs. 19 and 20. If, by measurement or mathematical analysis, the shape of  $R(t)$  can be determined, and if the output amplitude  $S$  for a unit step input is known, the signal/noise ratio of the shaper compared with other shapers is completely defined. (We neglect 1/f noise in this discussion.)

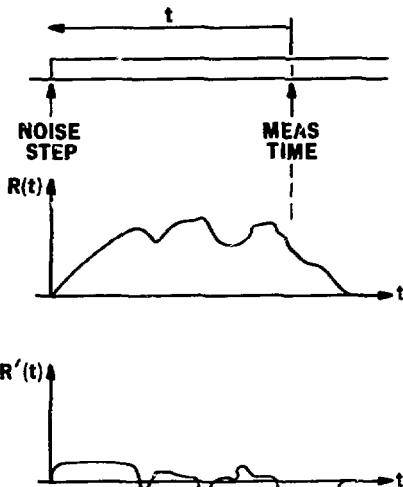


Fig. 14. Illustration of the behaviour of the noise residuals resulting from step and delta noise events at time  $t$  before the measurement time.

XBL 822-7924

## 5. THE TRAPEZOIDAL (TRIANGLE) SHAPE

While only approximately realizable a passive shaper producing a flat-topped triangular (trapezoidal) pulse shape provides a simple example of noise analysis in terms of  $R(t)$  and  $R'(t)$ . Figure 15 shows the steps involved in the analysis. The top portion of the figure shows the step response (and therefore the signal response in a semiconductor detector system) of the shaper. The  $R(t)$  function is derived as indicated in the second part of Fig. 15, by sliding the step response past the signal measurement time and plotting the residual response at the measurement time as a function of the time of origin of a noise pulse. This results in the  $R(t)$  function shown and differentiation produces the  $R'(t)$  function also shown. In the final part of the figure the  $R(t)$  and  $R'(t)$  functions are squared; since we have normalized all figures in terms of a peak amplitude of unity in the step response the evaluation of the noise indices (step and delta) involves simply determining the shaded areas in the last two parts of Fig. 15. Therefore:

$$\left. \begin{aligned} N_S^2 &= \tau_2 + (\tau_1 + \tau_3)/3 \\ N_\Delta^2 &= 1/\tau_1 + 1/\tau_3 \end{aligned} \right\} \quad (21)$$

If  $\tau_1 = \tau_3 = \tau_0$  and  $\tau_2 = 0$  (i.e. a symmetrical triangle)

$$\left. \begin{aligned} N_S^2 &= 0.67 \tau_0 \\ N_\Delta^2 &= 2/\tau_0 \end{aligned} \right\} \quad (22)$$

We note that the step noise index is proportional to  $\tau_0$  while the delta noise index is proportional to  $\tau_0^{-1}$ . Since these involve (noise)<sup>2</sup> the actual

signal/noise ratios involve  $(\tau_0)^{1/2}$ . We also note that, for this case, the  $R(t)$  function is the same as the signal. This is so for all passive shapers. Frequently the  $R(t)$  or "weighting" function is depicted reversed in the time direction. This does not affect the final result which relates only to the areas of

$$\{R(t)\}^2 \text{ and } \{R'(t)\}^2.$$

## 6. RC-RC INTEGRATOR DIFFERENTIATOR - TIME DOMAIN ANALYSIS

This type of shaper was analyzed in the frequency domain in section IV (3). The analysis resulted in absolute relationships for the noise given in Eqs. 17 and 18 which were then used to produce absolute noise values for the case shown in Fig. 13. By analyzing this shaper in the time domain we can directly compare its performance with others (such as the trapezoidal shaper) and the absolute performance, derived in the frequency domain calculation, can provide the base for absolute values for all other shapers analyzed in the time domain. This latter step is a convenience—absolute noise values can be obtained purely by time domain analysis as shown by Deighton.<sup>2</sup>

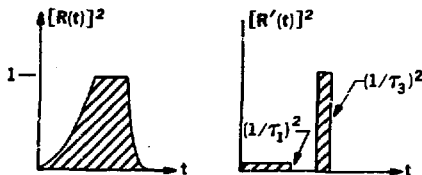
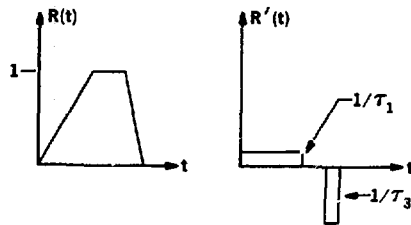
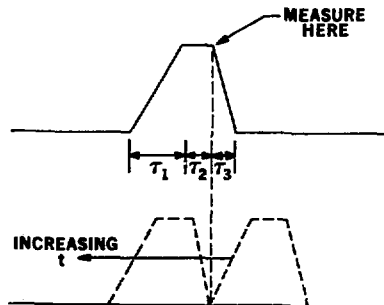
For the RC-RC Shaper:

$$R(t) = (t/\tau_0) e^{-(1-t/\tau_0)}$$

$$R'(t) = (\tau_0 - t)/\tau_0^2 e^{-(1-t/\tau_0)}$$

$$N_S^2 = \int_0^\infty (t/\tau_0) e^{-(1-t/\tau_0)} dt = 1.87 \tau_0 \quad (23)$$

$$N_\Delta^2 = \int_0^\infty (\tau_0 - t)/\tau_0^2 e^{-(1-t/\tau_0)} dt = 1.87/\tau_0 \quad (24)$$



XBL 822-7933

Fig. 15. Development of the noise indices for a trapezoidal pulse shaper.

An immediate comparison can now be made between the results for the RC-RC shaper and for the trapezoidal shaper. Table 2 compares the results for the RC-RC shaper with those for the symmetrical triangle. Since we can arbitrarily choose  $\tau_0$  (i.e., the peaking time) to be different for the two shapers, we can choose a larger value for the triangle and reduce its delta noise well below its value for the RC-RC shaper while the step noise remains much better for the triangle.

The final line in the table ( $\sqrt{N_S^2 N_\Delta^2}$ ) is a good index of noise performance with free choice of  $\tau_0$ . In this case we see that the triangle is over 60% better which could mean an improvement of 30 to 40% in signal/noise.

Table 2. Noise Indices for RC-RC and Symmetrical Triangler Shapers

	RC-RC	Triangle
$\overline{N_S^2}$	$1.87 \tau_0$	$0.67 \tau_0$
$\overline{N_\Delta^2}$	$1.87/\tau_0$	$2/\tau_0$
$\sqrt{\overline{N_S^2} \overline{N_\Delta^2}}$	1.87	1.16

In addition to the noise advantage, the triangular pulse shape returns to the baseline in  $2\tau_0$  while the RC-RC shape is only down to 30% of its peak amplitude at this time. In fact the long tail on the RC-RC pulse shape exists for many times  $\tau_0$ , and its pile-up behaviour at high counting rates is very poor.

Several conclusions can be drawn from this simple comparison:

- Choice of the pulse shaper can radically affect the noise and rate performance of a system. We note that these factors are intimately linked and both must be taken into account in a reasonable assessment of shapers.
- Symmetrical shapes are preferred. This is illustrated by considering the trapezoidal shape of Section IV (5). Here Eq. 21 can be rewritten with  $\tau_2 = 0$  and  $\tau_3 = \tau - \tau_1$  where  $\tau$  is the total pulse width:

$$\left. \begin{aligned} \overline{N_S^2} &= (\tau_1 + \tau_3)/3 = \tau/3 \\ \overline{N_\Delta^2} &= 1/\tau_1 + 1/\tau_3 = \tau/[\tau_1(\tau - \tau_1)] \end{aligned} \right\} (25)$$

While the step noise is independent of symmetry it is easy to show that  $\overline{N_\Delta^2}$  is a minimum when  $\tau_1 = \tau/2$ . In

fact,  $\overline{N_\Delta^2}$  rises to infinity as  $\tau_1 \rightarrow 0$ . This shows that the delta noise is primarily produced by fast rising (or falling) parts of  $R(t)$  and such fast transients are to be avoided if  $\overline{N_\Delta^2}$  is to be minimized.

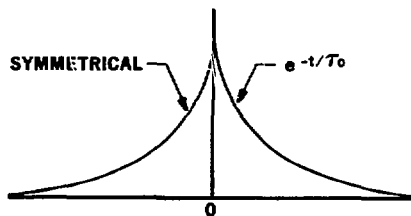
### 7. SYMMETRICAL CUSP SHAPE

It has long been known that the symmetrical cusp shape shown in Fig. 16 represents the ideal shape if signal/noise is the only consideration and if operation at a measurement time corresponding to the noise

minimum is acceptable (i.e., equal step and delta contributions). The cusp shape is represented by the function  $e^{-t/\tau_0}$  reflected about the  $t = 0$  ordinate. We have:

$$\left. \begin{aligned} \overline{N_S^2} &= 2 \int_0^\infty (e^{-t/\tau_0})^2 dt = \tau_0 \\ \overline{N_\Delta^2} &= 2/\tau_0^2 \int_0^\infty (e^{-t/\tau_0})^2 dt = 1/\tau_0 \\ \sqrt{\overline{N_S^2} \overline{N_\Delta^2}} &= 1 \end{aligned} \right\} (26)$$

The combined noise index for this shape is unity and it has long represented a target in the development of pulse shapers. Close approximations to the cusp shape for  $R(t)$  have been achieved using both passive and time variant shapers. Actually, for the great majority of spectroscopy systems, the long tails on the cusp shape are unacceptable as is the sharp peak.



XBL 822-7925

Fig. 16. A "cusp" shaped signal.

### 8. GAUSSIAN PULSE SHAPERS

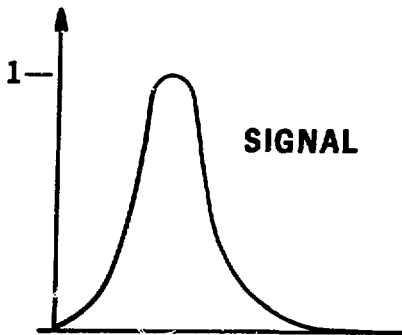
At the present time the most common pulse shape employed in spectroscopy systems is the Gaussian shape achieved by cascading one RC differentiator and several RC integrators. Usually so called "active" integrators are employed and by suitable design of these somewhat more symmetrical shapes can be achieved than are possible using pure RC integrators. The multiple RC integrator shape (Fig. 17) has the form

$$R(t) = (t/\tau_0)^n e^{n(1-t/\tau_0)} \quad (27)$$

Using this relationship and setting  $n = 2$  we have:

$$\left. \begin{aligned} \overline{N_S^2} &= 0.67 \tau_0 \\ \overline{N_\Delta^2} &= 2.53/\tau_0 \\ \sqrt{\overline{N_S^2} \overline{N_\Delta^2}} &= 1.30 \end{aligned} \right\} (28)$$

We note that this result is significantly worse than the symmetrical triangle ( $\sqrt{N_S^2 + N_A^2} = 1.30$  versus 1.16), but the Gaussian shape is easy to achieve with stable components and simple circuits.



XBL 822-7926

Fig. 17. A "Gaussian" shaped signal.

#### 9. INSENSITIVITY TO DETECTOR PULSE RISE TIME FLUCTUATIONS

We will digress briefly at this point to remind readers that in some cases (particularly large coaxial germanium gamma-ray spectrometers), the rise time variations in detector signals may become very significant and an important factor in the choice of a shaper may be its insensitivity to these variations. This means that the step function response of the shaper must exhibit a relatively flat top over a time at least equal to the maximum detector signal rise time. Shapers producing a sharply peaked waveform (such as the cusp) are not acceptable. Some shapers, such as the symmetrical triangle or the cusp may be modified to produce a flat top at a slight cost in the step noise index (note: since  $R'(t)$  is zero during the flat top, no penalty occurs in the delta noise index). The gated integrator, which will now be discussed, exhibits outstanding insensitivity to detector pulse rise time fluctuations and it is our first time variant system. Here, the shapes of  $R(t)$  and the step response are not the same because shaping elements are switch synchronously with the signal.

#### 10. GATED INTEGRATOR SHAPER

The circuit of this type of shaper is shown at the top of Fig. 18. In the particular implementation shown here, a Gaussian shaped signal is provided at the input of the integrator. At the start of a signal (detected in a parallel fast channel) switch S1 is closed and S2 is opened so that the feedback capacitor acts as an integrator for the signal. On the tail end of the Gaussian, S1 is opened thereby stopping further signal integration; by leaving S2 open for a short readout time following the opening of S1, a flat topped output signal is provided for any later output or digitizing process. Figure 18 shows the

time relationship between various waveforms and the switch operations. It also shows the  $R(t)$  function; the reader should attempt to derive this and should note the major difference between  $R(t)$  and the step function response.

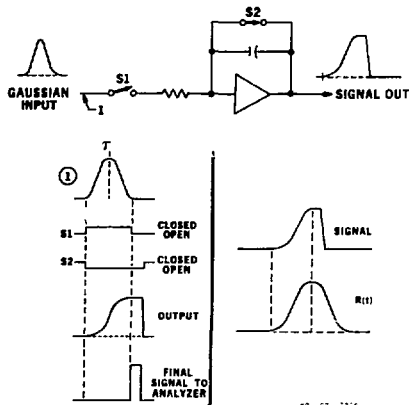
For a 7th order Gaussian (i.e.,  $n = 7$  in Eq. 27) the noise parameters can be calculated:

$$\left. \begin{aligned} \frac{N_S^2}{N_A^2} &= 2.07 \tau_0 \\ \frac{N_S^2}{N_A^2} &= 1.47/\tau_0 \\ \sqrt{N_S^2 + N_A^2} &= 1.74 \end{aligned} \right\} \quad (29)$$

We note that the overall noise figure of merit is substantially worse than the 7th order Gaussian

( $\sqrt{N_S^2 + N_A^2} = 1.30$ ), but for cases where the delta noise is dominant (e.g., where rate considerations force

operation at short pulse lengths), the value of  $N_A^2$  is much better (1.47/ $\tau_0$  versus 2.53/ $\tau_0$ ). Also, we have already noted the insensitivity to detector signal rise time; in Fig. 18 it is easy to see that a small time shift in the time components of the signal will only slightly affect the final output amplitude if the integration time extends to the tail end of the Gaussian-shaped pulse.



18. 62c-7926

Fig. 18. Development of the noise indices for a gated integrator.

#### 11. "HARWELL" PULSE PROCESSOR

A time-variant system designed to approach the performance of the cusp has been devised by the Harwell group led by K. Kandiah. The basic circuit is shown in Fig. 19, together with the output wave-shape and the  $R(t)$  function. The gated integrator behaves in the same way as described in the previous section, but, in this case, it is fed by an RC integrated waveform which is ac coupled on a long time constant to the gated integrator. A clamping switch

holds the input of the gated integrator at ground potential until a signal is sensed in the parallel fast channel. As optimized by Harwell, the integration time  $\tau_i$  is chosen to be twice the time constant  $\tau_1$  of the RC integrator.

Under these conditions the noise parameters are:

$$\left. \begin{aligned} \overline{N_S^2} &= 0.48 \tau_i \\ \overline{N_A^2} &= 2.1/\tau_i \\ \sqrt{\overline{N_S^2} \overline{N_A^2}} &= 1.03 \end{aligned} \right\} \quad (3D)$$

We note how closely this approaches the unity overall noise index exhibited by the cusp of Section IV (7).

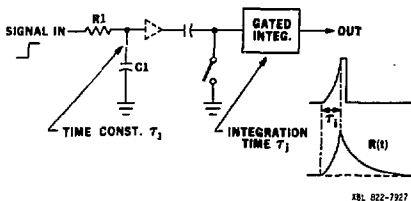


Fig. 19. The "Harwell" signal processor system.

Several modifications to this basic scheme are used in the actual processor to improve the insensitivity to detector pulse rise time and to limit the duration of the  $R(t)$  function. These include:

- i)  $R1$  is switched to infinity until the detector signal rise time  $\tau_r$  is complete. This eliminates rise time effects.
- ii) The gated integrator (as in Section IV (10)) retains its charge for a time  $\tau_A$  to permit readout of the signal.
- iii)  $R1$  is switched to a very small value at the end of  $\tau_A$  to discharge  $C1$ .

These changes result in the modifications to the  $R(t)$  function shown in Fig. 20.

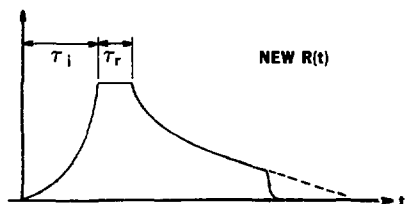


Fig. 20. Modifications to the  $R(t)$  function for the "Harwell" processor.

XBL 822-7928

A later section of the paper will relate the Harwell processor to other types of pulse shaper and will attempt to give some perspective on their behaviour.

## V. RATE CONSIDERATIONS - PILE-UP REJECTION

A system exhibiting optimum signal/noise ratio but with low signal throughput would be useful only in very few applications. Therefore, a compromise must always be made between rate and noise performance. The choice becomes somewhat more complicated when we include the fact that detector charge production statistics (see II (2)) determine the resolution at high energies; therefore, in high energy applications, degradation of noise performance can be tolerated if rate performance can be improved.

Virtually every spectrometer employs a pile-up rejector system to eliminate those pulses whose amplitude may be changed by accidental pile up. To discuss the system throughput (i.e., the rate at which "clean" pulses reach the output) we must understand the operation of pile-up rejectors.

### 1. PILE-UP REJECTION

Figure 21 shows a common type of pile-up rejection system. It uses narrow signals developed in an "inspection" channel which parallels the slow shaping channel used for pulse-height analysis. Signals in this channel which exceed a low level (set just above noise) trigger a fast discriminator which produces short logic signals. Following each such signal an inspection period is generated. The small delay in triggering the updating one-shot producing this inspection period prevents the narrow discriminator signal from setting the pile-up flip-flop via its input AND gate; however, if a second signal arrives before the end of the inspection period, it will trigger the pile-up flip-flop and the signal in the slow amplitude-measuring channel will be gated off thereby preventing its analysis. The waveforms in Fig. 21 illustrate this operation.

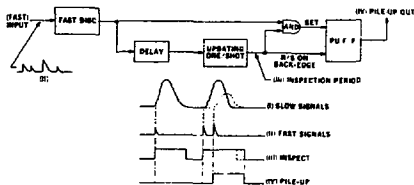


Fig. 21. Illustrating the basic operation of a typical pile-up rejector.

Several important points should be noted:

#### i) Resolving Time

The pulse width in the fast signal inspection channel limits the ability of the fast discriminator to recognize two very closely spaced signals. Such signals are very closely spaced

(~ 100 ns) so the associated events will appear as sum peaks in the analyzed slow channel pulse height spectrum. For example, if the resolving time in the inspection channel is 300 ns and the counting rate is 30 kHz about 1% of the counts will appear in sum peaks.

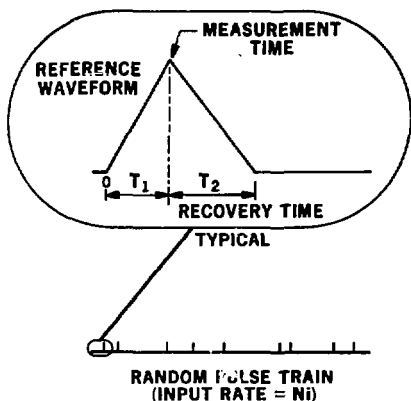
ii) Noise Threshold

Since the fast channel must employ very short integration times, a large amount of delta noise will be present and this will result in the need for the fast discriminator level to be set rather high. Pile-up of signals whose amplitude (in the fast channel) is lower than the fast discriminator threshold will, of course, not be detected.

For example, suppose a system exhibits ~ 150 eV FWHM noise resolution at 10  $\mu$ s shaping time in the slow channel. If the fast channel shaping times are in the 200 ns range we would expect the FWHM noise in the fast channel to be about 1 keV. To reduce noise triggering to a reasonable rate the fast discriminator threshold must be set to approximately 2 x FWHM noise level (= 2 keV). This simple calculation, which is reasonable close to the situation in X-ray spectrometers, illustrates one compromise involved in pile-up rejectors.

iii) Losses due to pile-up rejection

Figure 22 illustrates the situation occurring in a random pulse sequence in a spectroscopy system. For simplicity we assume each signal to be a triangle rising in time  $T_1$  and returning to the baseline in time  $T_2$  after a measurement at the peak. This can be generalized to include any signal measured  $T_1$  after its start, with a recovery time  $T_2$  after measurement.



XBL 822-7929

Fig. 22. A random sequence of triangular pulses.

Let  $p$  be the probability of an interval between two pulses being  $< t$

Then, the probability of an interval  $> t = 1-p$

If we increase  $t$  by  $dt$ , the increase  $dp$  in  $p$  will be:

$$dp = (1-p) N_i dt$$

where  $N_i$  is the input pulse rate. Integrating this equation:

$$p = 1 - e^{-N_i t} \quad (31)$$

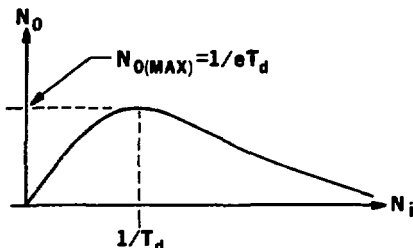
This equation can be used to calculate the throughput of various systems that use pile-up rejectors to reject pulses that are close together in time.

CASE 1: Reject a pulse if it is preceded by another in an interval  $< \tau_d$

probability of interval  $> \tau_d = 1-p = e^{-N_i \tau_d}$

$$\text{Output Rate} = N_i e^{-N_i \tau_d}$$

This relationship is shown in Fig. 23; we note that the peak output rate  $1/(\tau_d e)$  is achieved at an input rate  $1/\tau_d$ .



XBL 822-7930

Fig. 23. Plot of output versus input rate when using a pile-up rejector with an effective dead time of  $\tau_d$ .

CASE 2: Reject a pulse if its start is preceded by one in  $(T_1 + T_2)$  and also reject it if followed by one in  $T_1$ . This is the case in practically all pile up rejectors used in spectroscopy systems.

This is equivalent to Case 1 except that the effective value of  $\tau_d$  is  $2T_1 + T_2$ . For the special case where  $T_1 = T_2$  and  $T_1 + T_2 = T_W$  (the total pulse width) it is apparent that  $\tau_d = 1.5 T_W$ . This result which may surprise many, means that the dead time for loss calculations is 50% greater than the pulse width.

CASE 3: In the case of a gated integrator, as shown in Fig. 24, we can write

$$\begin{aligned} T_1 &= \tau_i && \text{for ideal case} \\ T_2 &= 0 \end{aligned}$$

This produces the unexpected result that  $T_D = 2 \tau_i$

In the general case we see that use of a standard type of pile up rejector results in an effective dead time  $T_d$  that is given by:

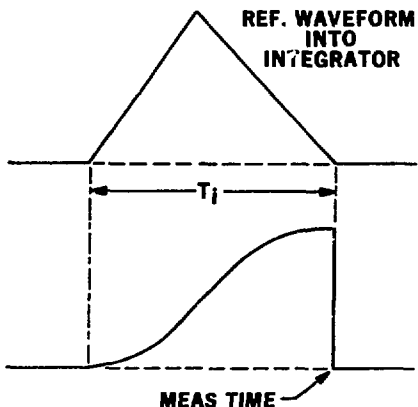
$$T_d = 2x (\text{Measurement Time}) + \text{Recovery Time}$$

The question might be asked whether the excessive loss penalty caused by normal pile-up rejectors cannot be avoided. In fact, at the cost of some circuit complications, it is possible to reduce  $T_D$  to equal to the sum of the measurement and recovery times. This will be the subject of a separate paper to be published in the near future.

#### VI. A PERFORMANCE COMPARISON

As indicated earlier several types of shapers are serious candidates for use and, while one may be advantageous under some circumstances, another might be preferred under different conditions. Complexity of circuit implementations, sensitivity to low frequency noise (such as ripple on power supplies or microphony) must be considered as well as the more basic criteria of performance. In some applications, (e.g., high energy particle spectroscopy) extraneous factors such as the spread in beam energy may be the dominant factor in determining energy resolution. Despite the diversity of this multiparameter problem, a good reference point must involve consideration primarily of the trade-off between electronic resolution and signal throughput at high counting rates. Therefore, for our comparison, we have chosen to present the results in Table 3, first in terms of the noise indices, then, toward the bottom of the table, we have expressed the behavior of the delta noise

index (which will nearly always be dominant in systems designed to perform at high rates) in terms of the "throughput" dead time  $T_D$ . To compute  $T_D$ , we have assumed that the inspection time of a normal pile-up rejector is set to a value where the shaped signal has recovered to 0.1% of its peak amplitude.



XBL 822-7931

Fig. 24. Illustrating the pile-up behaviour of a gated integrator system.

Table 3. Comparison of the Performance of Some Pulse Shapers

	Triangle	RC-RC Integ/Diff	7th Order Gaussian	+ Gated Integ	Harwell
$\overline{N_s^2}$	$0.67 \tau_0$	$1.87 \tau_0$	$0.67 \tau_0$	$2.075 \tau_0$	$0.48 \tau_i$
$\overline{N_d^2}$	$2/\tau_0$	$1.87 \tau_0$	$2.53/\tau_0$	$1.47/\tau_0$	$2.1 \tau_i$
$\sqrt{\overline{N_s^2} \overline{N^2}}$	1.16	1.87	1.30	1.74	1.03
$T_D$	$3 \tau_0$	$11 \tau_0$	$4.1 \tau_0$	$5 \tau_0$	$\sim 3.5 \tau_i$
$\overline{N_d^2}$	$6/T_D$	$20/T_D$	$9.4/T_D$	$7.35/T_D$	$7.35/T_D$

As indicated by the results in the final line of Table 3, substantial improvements in the product

$\overline{N_A^2} \cdot T_D$  can be realized by choosing the right shaper. It is interesting that the best shaper on this basis, the symmetrical triangle, has hitherto not been used because of the apparent difficulties in generating the shape. It is also of interest to note that the use of a more complex pile-up rejector as discussed earlier can reduce the effect in value for  $T_D$  by as much as 33% for the passive shapers (with no change for the gated integrator and Harwell processor). Therefore,

in this case the product  $\overline{N_A^2} \cdot T_D$  for the symmetrical triangle becomes 4—making it the ideal system (under the terms of our comparison) by a wide margin.

## VI. CONCLUSION

The objective in this paper has to provide a reasonably detailed view of the subject of processing signals from detectors and to indicate the factors which should enter into the choice of an optimum system for a given application. Together with other papers given in this Short Course, we hope that the reader will obtain a fairly comprehensive picture of the whole field of semiconductor detector spectroscopy.

## VII. ACKNOWLEDGMENTS

The authors are particularly indebted to Norman Madden whose constant inquisitiveness regarding these problems has stimulated much of the thinking that forms the heart of this paper. We also wish to thank Paul Phelps and members of the IEEE Nuclear Science Symposium whose continuing interest in this Short Course makes our presentation possible.

This work was supported by the Director's Office of Energy Research, Office of Health and Environmental Research Pollutant Characterization and Safety Research Division of the U. S. Department of Energy under Contract No. DE-AC03-76SF00098

## VIII. REFERENCES

1. Landis, D.A., Cork, C.P., Madden, N.W. and Goulding, F.S., "Transistor Reset Preamplifier for High-Rate High-Resolution Spectroscopy", Lawrence Berkeley Laboratory Report LBL-13214 (to be published in IEEE Trans. Nucl. Sci. NS-29, Feb. 1982).
2. Deighton, M. D., Nucl. Instr. and Methods 58, 201 (1968).